

Electron density and recombination rate measurements in CO-seeded optically pumped plasmas

Peter Palm, Elke Plönjes, Matt Buoni, Vish V. Subramaniam, and Igor V. Adamovich^{a)}

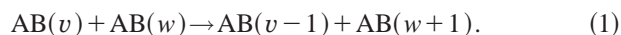
*Nonequilibrium Thermodynamics Laboratory, Department of Mechanical Engineering,
The Ohio State University, Columbus, Ohio 43210-1107*

(Received 8 December 2000; accepted for publication 8 February 2001)

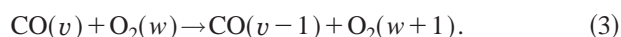
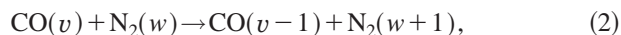
Electron production rate and electron density in cold optically pumped CO–Ar and CO–N₂ plasmas in the presence of small amounts of O₂ and NO have been measured using a Thomson discharge probe and microwave attenuation. Nonequilibrium ionization in the plasmas is produced by an associative ionization mechanism in collisions of highly vibrationally excited CO molecules. It is shown that adding small amounts of O₂ or NO (50–100 mTorr) to the baseline gas mixtures at $P=100$ torr results in an increase of the electron density by up to a factor of 20–40 (from $n_e < 10^{10} \text{ cm}^{-3}$ to $n_e = (1.5\text{--}3.0) \times 10^{11} \text{ cm}^{-3}$). This occurs while the electron production rate either decreases (as in the presence of O₂) or remains nearly constant within a factor of 2 (as in the presence of NO). It is also shown that the electron–ion recombination rates inferred from these measurements decrease by two to three orders of magnitude compared to their baseline values (with no additives in the cell), down to $\beta \cong 1.5 \times 10^{-8} \text{ cm}^3/\text{s}$ with 50–100 mTorr of oxygen or nitric oxide added to the baseline CO–Ar mixture, and $\beta \cong (2 \text{ to } 3) \times 10^{-7} \text{ cm}^3/\text{s}$ with 75–100 mTorr of O₂ or NO added to the baseline CO–N₂ mixture. The overall electron–ion removal rates in the presence of equal amounts of O₂ or NO additives turn out to be very close, which shows that the effect of electron attachment to oxygen at these conditions is negligible. These results suggest a novel method of electron density control in cold laser-sustained steady-state plasmas and open a possibility of sustaining stable high-pressure nonequilibrium plasmas at high electron densities and low plasma power budget. © 2001 American Institute of Physics. [DOI: 10.1063/1.1359754]

I. INTRODUCTION

Steady-state nonequilibrium optically pumped environments are produced by resonance absorption of infrared laser radiation by molecules in low vibrational quantum states, with subsequent collisional vibration-to-vibration (V - V) pumping up to high vibrational levels,^{1,2}

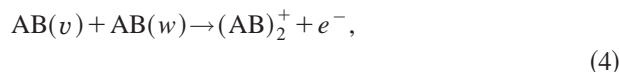


In Eq. (1), AB stands for a diatomic molecule, and v and w are vibrational quantum numbers. This method creates strong vibrational disequilibrium at high densities (up to a few atm in the gas phase), wide temperature range ($T=100\text{--}1500$ K), and a low power budget ($\sim 1\text{--}10 \text{ W/cm}^3$). In particular, optical pumping by a CO laser has been previously achieved in gas phase CO/Ar/He mixtures^{3–8} at pressures of up to 10 atm,³ gas phase nitric oxide,^{9,10} liquid phase CO,^{11,12} and solid CO and NO matrices.^{13,14} Recently, optical pumping has also been demonstrated in mixtures of CO with infrared inactive gases, such as nitrogen and air, at atmospheric pressure.^{15,16} In this case, N₂ and O₂ molecules become vibrationally excited by near-resonance V - V energy transfer from CO,



In the experiments of Refs. 2–16, the CO laser power was fairly low, ranging from a few watts to 200 W cw.

Ionization in optically pumped gases is produced by an associative ionization mechanism in collisions of two highly vibrationally excited molecules when the sum of their vibrational energies exceeds the ionization potential,^{17–20}



$$E_v + E_w > E_{\text{ion}}.$$

Ionization of carbon monoxide by this mechanism has been previously observed in CO/Ar/He gas mixtures optically pumped by resonance absorption of CO laser radiation.^{18–20} The estimated steady-state electron density sustained by a 10 W CO laser in optically pumped CO/Ar/He plasmas with high vibrational level populations of $n_{\text{CO}}(v \sim 30) \sim 10^{15} \text{ cm}^{-3}$ is $n_e \sim 10^{10}\text{--}10^{11} \text{ cm}^{-3}$.¹⁹ Note that unlike electron impact ionization, the ionization mechanism of Eq. (4) is not susceptible to the ionization heating instability, which is responsible for filamentation and the glow-to-arc collapse in high-pressure nonequilibrium plasmas, where ionization is primarily produced by electron impact.²¹ Indeed, since the high vibrational level populations of diatomic molecules decrease with temperature due to an exponential rise of the vibration-translation (V - T) relaxation rates,²² there is a negative feedback between the gas heating and the rate of associative ionization. This precludes the ionization instability development and provides a possibility for the use of

^{a)}Electronic mail: adamovich.1@osu.edu

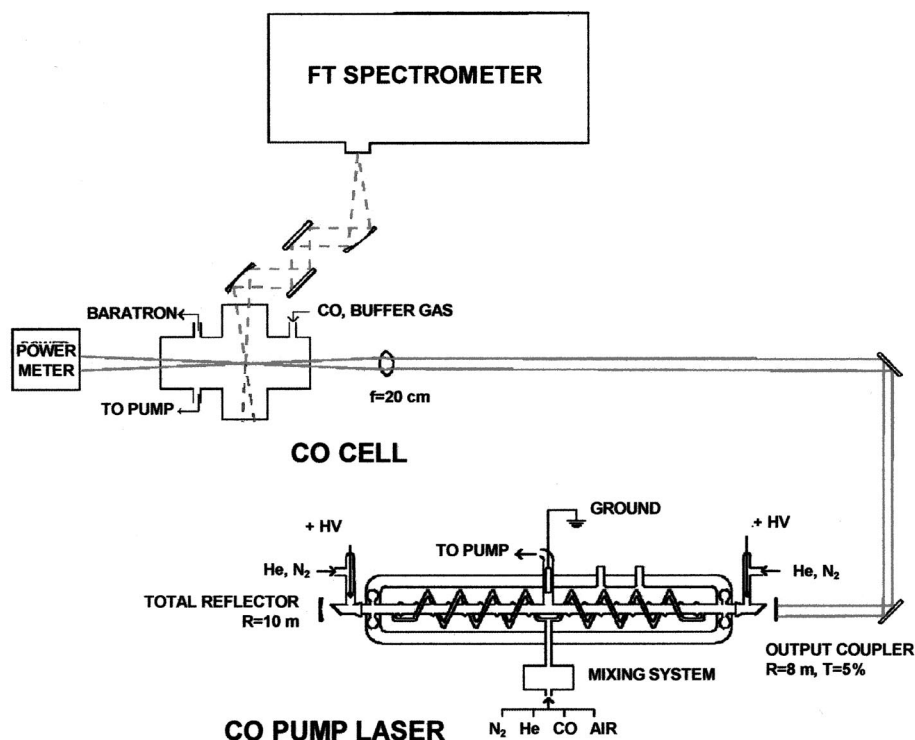


FIG. 1. Schematic of the experimental setup.

associative ionization for sustaining unconditionally stable optically pumped nonequilibrium plasmas at high gas pressures (1 atm and above).

The present article addresses the effect of adding air species, such as O₂ and NO, to optically pumped CO/Ar and CO/N₂ plasmas on the electron production and removal kinetics. Previous results²⁰ suggest that adding these species produces a significant electron density rise in these plasmas at a nearly constant plasma power budget and electron production rate. Therefore the main objective of the present study is to investigate the role of these additives on the electron density and on the electron removal rate in the plasma. This would provide insight into the feasibility of sustaining large-volume atmospheric pressure nonequilibrium air plasmas at a minimum power budget.

II. EXPERIMENT

The overall schematic of the experimental setup is shown in Fig. 1. A carbon monoxide laser is used to excite CO/Ar and CO/N₂ gas mixtures, with additives such as O₂ or NO, slowly flowing through the pyrex glass optical absorption cell shown. The residence time of the gas mixture in the cell is of the order of a few seconds. The liquid nitrogen cooled CO laser⁸ is designed in collaboration with the University of Bonn and fabricated at Ohio State. It produces a substantial fraction of its power output on the $v = 1 \rightarrow 0$ fundamental band component in the infrared. In the present experiment, the laser is typically operated at 10–13 W cw broadband power on the lowest ten vibrational bands. The output on the lowest bands ($1 \rightarrow 0$ and $2 \rightarrow 1$) is necessary to start the absorption process in cold CO (initially at 300 K) in the cell. The laser beam can be focused to a focal area of

~1 mm diameter to increase the power loading per CO molecule, producing an excited region 10–20 cm long and 2 to 3 mm in diameter.

The lower vibrational states of CO, $v \leq 10$, are populated by direct resonance absorption of the pump laser radiation in combination with rapid redistribution of population by V-V exchange processes. The V-V processes then continue to populate higher vibrational levels above $v = 10$, which are not directly coupled to the laser radiation [see Eq. (1)]. The large heat capacity of the Ar and N₂ diluents, as well as conductive and convective cooling of the gas flow, enables control over the translational/rotational mode temperature in the cell. At steady-state conditions, when the average vibrational mode energy of the CO would correspond to a few thousand degrees Kelvin, the temperature never rises above a few hundred degrees. Thus a strong disequilibrium of energy can be maintained in the cell, characterized by very high vibrational mode energy and a low translational/rotational mode temperature. As shown in Fig. 1, the population of the vibrational states of CO in the cell is monitored using a Biorad FTS 175C Fourier transform infrared spectrometer, which records spontaneous emission from the CO fundamental, first and second overtone bands through a CaF₂ window on the side of the cell.

Ionization of highly excited CO molecules in the cell occurs by the associative ionization mechanism of Eq. (4). The electron production rate in this optically pumped plasma is determined from the saturation current of the non-self-sustained dc Thomson discharge^{18–20} between two 3 cm diameter brass plate electrodes located in the absorption cell as shown in Fig. 2. Two infrared transparent CaF₂ windows were placed upstream and downstream of the plates (see Fig. 2) so that the laser beam creates a nearly cylindrical excited

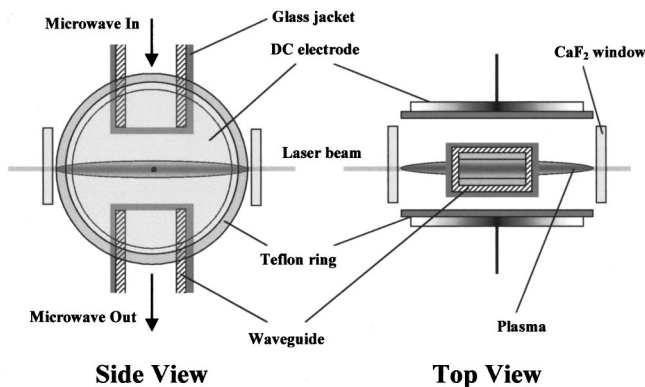


FIG. 2. Schematic of the Thomson discharge electrode and microwave waveguide arrangement in the absorption cell.

region between the windows. Thus the plasma generated in the interelectrode space is isolated from the plasma sustained in the remainder of the cell, which significantly reduces the charged species drift and diffusion into the interelectrode space. This allows reaching a well-pronounced current saturation. The electrodes, which are typically 10–20 mm apart, are connected to a reversible polarity dc power supply (Thorn EMI GENCOM Inc., model 3000R), which produces voltage in the range 0–3000 V. The induced current is measured with a Keithley 2001 multimeter, with a 1 MΩ resistor connected in series with the cell to protect the multimeter in case of breakdown. The applied dc voltage is deliberately kept sufficiently low to preclude electron impact ionization. Therefore in the saturation regime of the Thomson discharge, the applied electric field, which does not produce any ionization by itself, removes as many electrons per second as are produced in the entire discharge volume. The electron production rate per unit volume of the plasma is found from the saturation current as²⁰

$$S \cong \frac{I_s}{e\pi d^2 D/4}, \quad (5)$$

where d is the diameter of the ionized region created by the focused laser beam, D is the electrode diameter, and $\pi d^2 D/4$ is the volume occupied by the plasma. The plasma diameter, $d = 2.5 \pm 0.5$ mm, is estimated from the diameter of the visible blue glow of the C₂ Swan band radiation, which is strongly coupled with the high vibrational level populations of CO.⁷

The electron density in the optically pumped plasma is independently measured by microwave attenuation. The microwave experimental apparatus consists of an oscillator, a transmitting and receiving antenna/waveguide system, and transmitted and reflected microwave power detectors. The phase-locked dielectrically stabilized oscillator generates 20 mW (13 dBm) of microwave radiation at a frequency $\nu = 10$ GHz, which is transmitted via SMA-type semirigid cable to an antenna within the transmission waveguide. The gap between the waveguides is 1 cm. The receiving waveguide is positioned directly opposite the transmitting waveguide, with the laser-generated plasma located between them (see Fig. 2). The signal transmitted through the plasma is received by an antenna at the back of the receiving wave-

guide and sent to a tunnel diode detector with a low-noise preamplifier. The detector produces a low-noise dc voltage proportional to the received microwave power, ranging from 0 to 15 V for the transmitted power in the range from –60 to –30 dBm. The voltage noise level is typically 1 to 2 mV, so that the resultant signal-to-noise ratio is $\sim 10^4$. Power reflected by the plasma is detected by a zero-bias Schottky diode detector through an isolator in the line between the oscillator and the transmitting antenna. This detector produces a dc voltage in the mV range proportional to the reflected microwave power in the range from 0 to 20 mW. In the present experiments, the measured change in reflected power between the laser on and laser off conditions is negligible.

Typical microwave power levels transmitted across the 1 cm gap between the waveguides were in the range of –10 to 0 dBm, decreasing by up to 1 dB when the plasma was generated. To scale the transmitted signal down to the power range over which the detector has the highest sensitivity (that is, down to the –60 to –30 dBm range), attenuators were inserted in the line between the receiving antenna and the transmitted power detector. From the relative difference of the transmitted power with and without a plasma the attenuation of the microwave signal across the plasma was determined with an uncertainty of 0.002 dB. This assumes a negligible difference in the power radiated from the gap between the waveguides, with and without the plasma present, which is justified by the negligible change in the measured reflected power at these conditions.

During the microwave attenuation measurements, the laser beam was chopped at a frequency of 57 Hz, providing a square wave laser input into the cell. The laser remained on and off for approximately 8 ms. Our previous time-resolved Fourier transform infrared spectroscopy measurements⁸ showed that at CO partial pressures $P_{CO} > 0.5$ torr this time is sufficiently long to reach both the quasi-steady-state fully V - V pumped distribution and the complete vibrational relaxation of CO in the cell. In addition, the characteristic time scales for associative ionization and for electron–ion recombination, $\tau_{ion} \sim n_e / (k_{ion} n_{CO}^2 f_{v>30}^2) \sim 0.1$ ms, and $\tau_{rec} \sim 1/\beta n_e \sim 0.1$ – 1.0 ms are both much shorter than the chopper cycle duration. Here $k_{ion} = 1.5 \times 10^{-13}$ cm³/s is the associative ionization rate coefficient,²⁰ $n_{CO} = 10^{17}$ cm⁻³ is the CO concentration in the cell (at $P_{CO} = 3$ torr), $f_{v>30} \sim 10^{-3}$ is the fraction of the CO molecules participating in the associative ionization process of Eq. (4),²⁰ $\beta = 10^{-8}$ – 10^{-7} cm³/s is the electron–ion dissociative recombination rate, and $n_e = 10^{11}$ cm⁻³ is the estimated maximum electron density.²⁰ Therefore the laser on and laser off conditions correspond to the quasi-steady-state weakly ionized plasma and nearly fully recombined plasma conditions, respectively. The difference between the incident and transmitted microwave powers between the plasma on and plasma off conditions was determined from the amplitude of the resultant nearly square wave forward power detector signal, $\delta V = V_{inc} - V_{trans}$, modulated by the chopper, and averaged by a Tectronix TDS380 oscilloscope over 256 averages. The average electron density in the plasma was inferred from these measurements using the relation,²¹

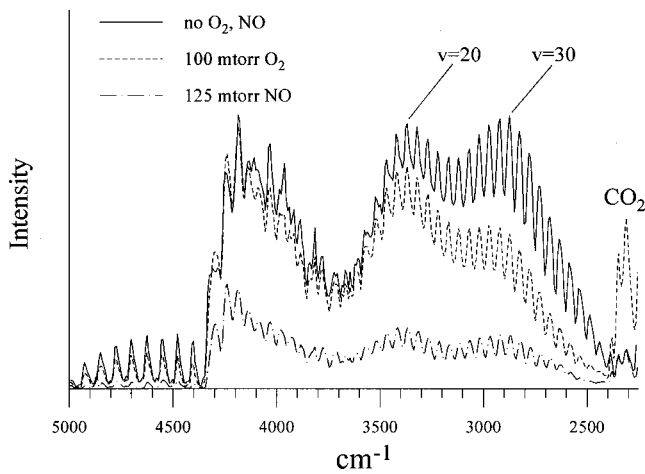


FIG. 3. First overtone CO emission spectra in optically pumped CO–Ar mixtures with small amounts of O₂ and NO added. $P_{\text{CO}}=3$ torr, $P_{\text{Ar}}=100$ torr.

$$n_e = \frac{m_e c \epsilon_0}{e^2} \nu_{\text{coll}} \frac{\delta V}{V_{\text{inc}}} \frac{1}{d} \frac{W}{d}, \quad (6)$$

where ν_{coll} is the electron–neutral collision frequency, $\delta V/V_{\text{inc}} = (V_{\text{trans}} - V_{\text{inc}})/V_{\text{inc}}$ is the relative attenuation factor in terms of the forward power detector voltage proportional to the incident and the transmitted microwave power, $W = 1$ cm is the waveguide width, and $d = 2.5 \pm 0.5$ mm is the diameter of the ionized region. The electron–neutral collision frequency in CO–Ar and CO–N₂ mixtures at $P = 100$ torr and $T = 600$ K, $\nu_{\text{coll}} = 1.1 \times 10^{12}$ cm³/s and $\nu_{\text{coll}} = 2.1 \times 10^{12}$ cm³/s, respectively, was obtained from the Boltzmann equation solution¹⁹ using the experimental cross sections of elastic and inelastic electron collision processes available in the literature.

O₂ or NO were both diluted in nitrogen at the 5000 ppm level to add controlled small amounts (from a few millitorr to a few hundred millitorr) of these species to the cell. The resultant O₂/N₂ and NO/N₂ gas mixtures have been added to the baseline CO/Ar and CO/N₂ gas mixtures. The baseline pressure in the cell was $P = 100$ torr, with the CO partial pressure of $P_{\text{CO}} = 3$ torr. The O₂/N₂ and NO/N₂ mixture partial pressure was varied from 1 to 100 torr. Note that adding the same amounts of pure nitrogen (without the additives) to the baseline gas mixtures did not produce significant changes in the measured electron density.

III. RESULTS AND DISCUSSION

Figure 3 shows the low-resolution (8 cm⁻¹) CO first overtone infrared emission spectra measured in the optically pumped CO–Ar plasmas with O₂ and NO additives. At these conditions, vibrational levels up to $v \sim 35$ –40 are populated and radiating. From Fig. 3 one can see that adding small amounts ($\sim 0.1\%$) of oxygen to the cell gases results in the depopulation of the high vibrational levels of CO ($v > 15$ –20), without producing significant changes in the low vibrational level populations. This is most likely due to the rapid near-resonance V–V energy transfer from highly excited CO to O₂,

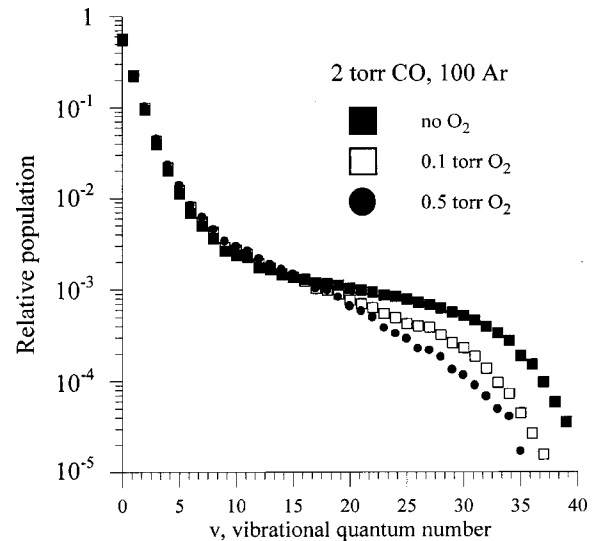
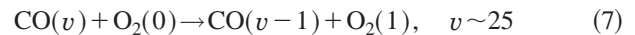
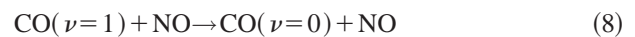


FIG. 4. CO vibrational level populations for the conditions similar to those of Fig. 3. $P_{\text{CO}}=2$ torr, $P_{\text{Ar}}=100$ torr.



as discussed in our previous publication.¹⁵ On the other hand, adding comparable amounts of nitric oxide to the baseline CO–Ar mixture, in addition to reducing the intensities of the high vibrational bands ($v' = 20$ –30) compared to the low bands ($v' = 2$ –5), decreases the absolute intensity of the entire spectrum (see Fig. 3). This indicates that the populations of all CO vibrational levels in the range $v \sim 2$ –35 are substantially reduced in the presence of NO. This is consistent with the fact that compared to CO and O₂, NO is a much faster V–T relaxer,²³ so that even the low vibrational levels of CO are depopulated by the rapid V–T relaxation processes such as



which are competing with the V–V pumping process of Eq. (1). Thus in both these cases, the concentration of the highly vibrationally excited CO molecules in the cell is reduced. Indeed, Fig. 4 illustrates this effect showing CO vibrational distribution functions inferred from the high-resolution (0.25 cm⁻¹) CO infrared spectra in CO–Ar–O₂ mixtures. Similar behavior has been previously observed from the CO distribution function measurements in CO–Ar–NO mixtures.²⁰ At these experimental conditions ($P = 100$ torr, $P_{\text{CO}} = 3$ torr), the translational/rotational mode temperature inferred from the high-resolution (0.25 cm⁻¹) infrared spectra is in the range of $T = 500$ –700 K.^{8,18,20}

Figure 5 displays the microwave signal intensity transmitted through an optically pumped CO–Ar–NO plasma. As discussed in Sec. II, the signal is modulated by a chopper providing a square wave laser input into the cell. It can be seen from Fig. 5 that turning on the laser results in the well-pronounced attenuation of the transmitted signal due to the vibrationally stimulated ionization in the cell.

Figures 6 and 7 show the average electron density in the optically pumped CO–Ar plasmas with small admixtures of O₂ and NO, respectively. One can see that in both cases

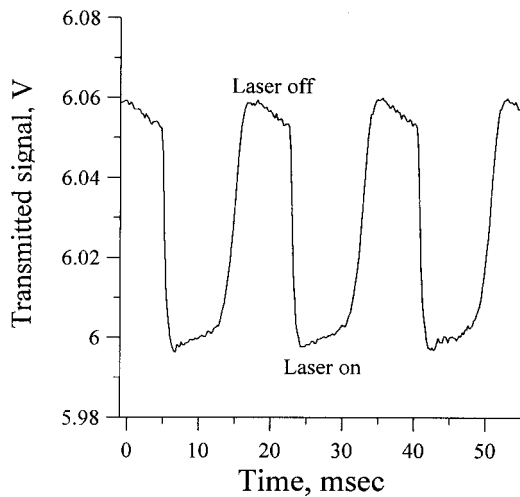


FIG. 5. Transmitted microwave signal with the pump CO laser turned on and off. $P_{CO}=3$ torr, $P_{Ar}=100$ torr, and $P_{NO}=50$ mTorr.

adding 50–75 mTorr of oxygen or nitric oxide to the cell gases increases the electron density by about a factor of 20–40, up to $n_e=(1.5-3.0)\times 10^{11}\text{ cm}^{-3}$, compared with the baseline case with only CO and Ar in the cell, $n_e=(3-6)\times 10^9\text{ cm}^{-3}$. This type of behavior is somewhat unexpected since oxygen is known to be an efficient electron attacher by a three-body process,



with a rate of $k_{att}N=10^{-11}\text{ cm}^3/\text{s}$,²⁴ which is likely to reduce the electron density. Further increase of the additive partial pressure up to 400–500 mTorr resulted in the gradual reduction of the electron density back to $n_e=(1\text{ to }2)\times 10^{10}\text{ cm}^{-3}$ (see Figs. 6 and 7). The uncertainty in the measured electron density, indicated by the error bars in Figs. 6 and 7 is mostly due to uncertainty in the diameter of the ionized region, estimated to be in the range between 2.0 and 3.0 mm (see Sec. II). The measured maximum electron densities are consistent both with the values predicted by coupled master equation/Boltzmann equation modeling

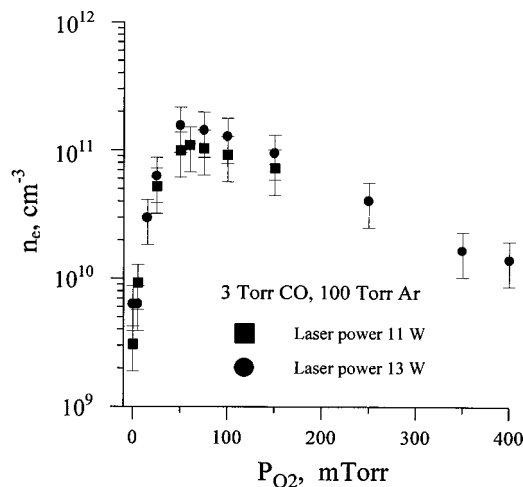


FIG. 6. Electron density in CO–Ar–O₂ mixtures as a function of the O₂ partial pressure.

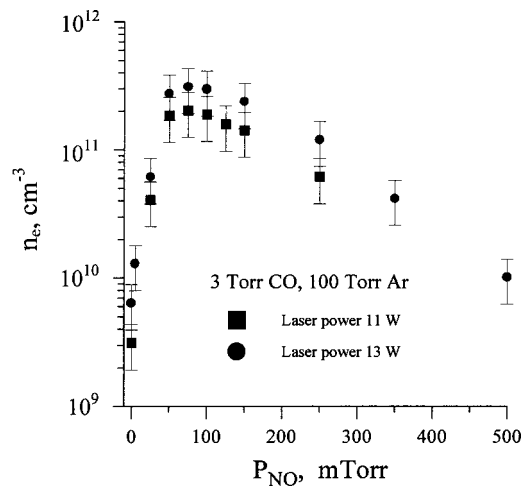


FIG. 7. Electron density in CO–Ar–NO mixtures as a function of the NO partial pressure.

calculations¹⁹ and inferred from rf probe conductivity measurements.²⁰ Similar behavior of electron density as a function of additive partial pressure was observed in CO/N₂/O₂ and CO/N₂/NO mixtures (see Fig. 8), where the electron density also increased by about a factor of 10–20 in the presence of 25–75 mTorr O₂ or NO.

The observed sharp electron density rise with the additive partial pressure between 0 and 100 mTorr (see Figs. 6 and 7) occurs despite the fact that the CO vibrational level populations have been found to monotonously decrease when oxygen or nitric oxide are added to the cell (see Figs. 3 and 4 and Ref. 20). This rise might be interpreted by the participation of O₂ and NO molecules, which both have lower ionization potentials than CO (12.1, 9.6, and 14.0 eV, respectively), in the vibrationally stimulated ionization process of Eq. (4). However, measurements of the net electron production rate at these conditions turn out to be inconsistent with this suggestion. Figure 9 shows current–voltage characteristics of the Thomson discharge sustained between two dc electrodes in the CO–Ar–O₂ plasma (see Fig. 2). One can see that the saturation current of this discharge, proportional

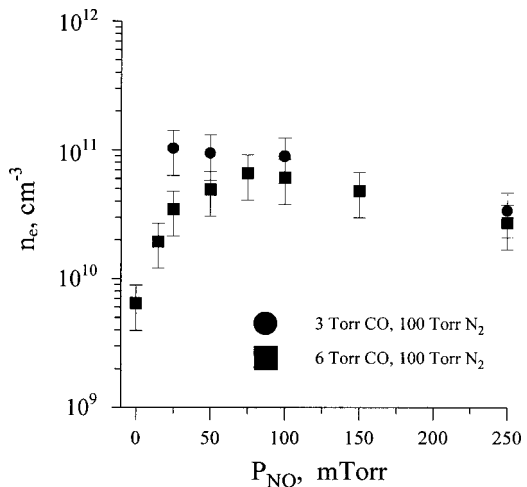


FIG. 8. Electron density in CO–N₂ mixtures as a function of the NO partial pressure.

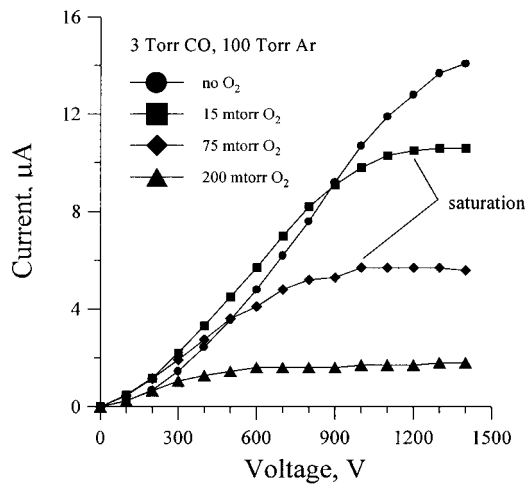


FIG. 9. Saturation of the Thomson discharge in the optically pumped CO-Ar-O₂ mixtures.

to the electron production rate in the plasma, is actually dropping with the O₂ concentration. As discussed in Sec. II, in the saturation regime, the applied electric field removes as many electrons per second as are produced in the entire discharge volume. This is illustrated by the measurements of electron density in the Thomson discharge as a function of the applied voltage (see Fig. 10). The fact that the electron density in the plasma drops by about an order of magnitude as the discharge approaches saturation confirms that the saturation current indeed approaches the net electron production rate (within about 10%).

The independent measurements of the electron density and the electron production rate lead us to conclude that the simultaneous electron production rate drop and electron density rise with the additive partial pressure can be only due to the net electron removal rate reduction in the presence of small amounts of O₂ or NO (up to 100 mTorr) in the optically pumped CO-Ar and CO/N₂ plasmas.

To infer the electron removal rate in the optically pumped plasmas, we measured both the electron production rate and the electron density in the same experiment. At

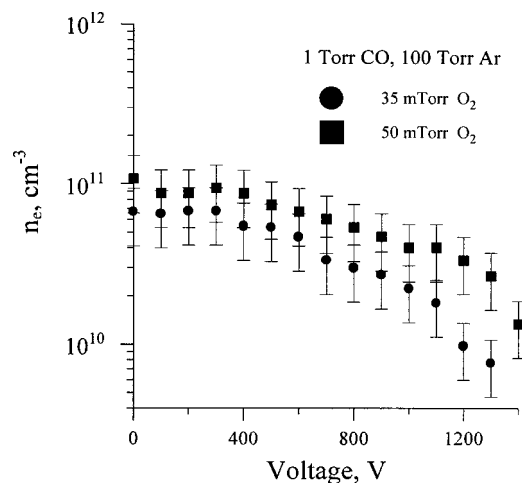


FIG. 10. Electron removal by the applied field in the Thomson discharge approaching saturation.

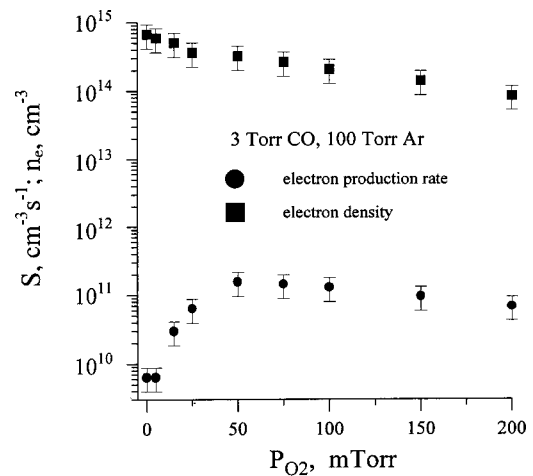


FIG. 11. Electron production rate and electron density in CO-Ar-O₂ mixtures as a function of O₂ partial pressure.

these conditions, the electron removal rate is essentially a sum of three processes, (i) ambipolar diffusion of charged species out of the ionized region, (ii) electron-ion recombination, and (iii) electron attachment to oxygen molecules. The time scales for the electron removal by the first two mechanisms differ by about an order of magnitude, $\tau_{\text{diff}} \sim d^2/D_a \sim 10$ ms and $\tau_{\text{rec}} \sim 1/\beta n_e \sim 0.1-1.0$ ms, where $d \sim 0.2$ to 0.3 cm is the diameter of the ionized region, $D_a \sim 5$ cm²/s is the ambipolar diffusion coefficient at $P = 100$ torr,²⁵ $\beta \sim 10^{-8}-10^{-7}$ cm³/s is the dissociative recombination coefficient, and $n_e \sim 10^{11}$ cm⁻³ is the electron density. Therefore in the present work we neglect charge species loss by diffusion. Also, O₂⁻ ion formation by the three-body electron attachment process of Eq. (9) is neglected. The arguments in favor of this assumption are as follows: (i) adding small amounts of O₂ to the cell gases results in an increase of the electron density in the plasma, which suggests that rapid three-body electron attachment to oxygen is mitigated to a large extent, (ii) similar results were obtained when comparable amounts of NO, which is not an efficient electron attacher, are added to the cell gases, and (iii) Raman spectroscopy measurements of the O₂ vibrational level populations ($v=0-12$) in the optically pumped CO/N₂/O₂ plasmas^{15,16} show that O₂ in these mixtures becomes strongly vibrationally excited, reaching a vibrational temperature of $T_v(\text{O}_2) = 2200-3600$ K. In particular, the latter result suggests that strong vibrational excitation of O₂ might well stimulate detachment of electrons from the weakly bound O₂⁻ ions (with an electron affinity of ~ 0.43 eV).

With the dominant electron removal process being dissociative recombination, in the steady state its rate can be directly inferred from the electron production rate per unit volume, S , and the electron density, n_e ,

$$\beta = \frac{S}{n_e^2}. \quad (10)$$

Figures 11 and 12 show the results of simultaneous measurements of the electron production rate inferred from the Thomson discharge saturation current and the electron density in the optically pumped CO-Ar-O₂ and in CO-Ar-NO

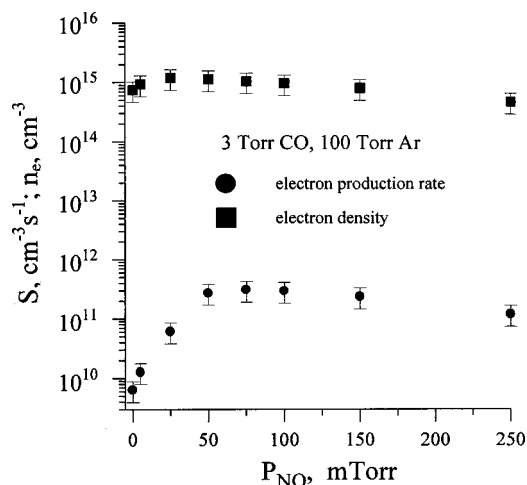


FIG. 12. Electron production rate and electron density in CO–Ar–NO mixtures as a function of NO partial pressure.

mixtures, respectively. From Fig. 11, one can see that the electron production rate drops with the O₂ partial pressure by about a factor of 5, while electron density increases by approximately a factor of 30. Similarly, Fig. 12 shows that the electron production rate weakly changes (approximately within a factor of 2) depending on the NO partial pressure, while the electron density increases with the NO partial pressure almost by a factor of 50. Figure 13 shows the electron–ion recombination rate coefficients inferred from these data using Eq. (10). It can be seen that the recombination rate in CO–Ar–O₂ and in CO–Ar–NO mixtures decreases by about three orders of magnitude, from its baseline value of $\beta = 2 \times 10^{-5} \text{ cm}^3/\text{s}$ (with no additives in the cell) to $\beta \sim 1.5 \times 10^{-8} \text{ cm}^3/\text{s}$ with 50–100 mTorr oxygen or nitric oxide added (see Fig. 13). Interestingly, the electron–ion recombination coefficients in both mixtures (with 50–100 mTorr of O₂ or NO added) are very close, which shows that the contribution of electron attachment to oxygen at these conditions is negligible. Similarly, the recombination rate in CO–N₂–O₂ and CO–N₂–NO mixtures decreases by about two orders of magnitude, from $\beta = 5 \times 10^{-5} \text{ cm}^3/\text{s}$ with no

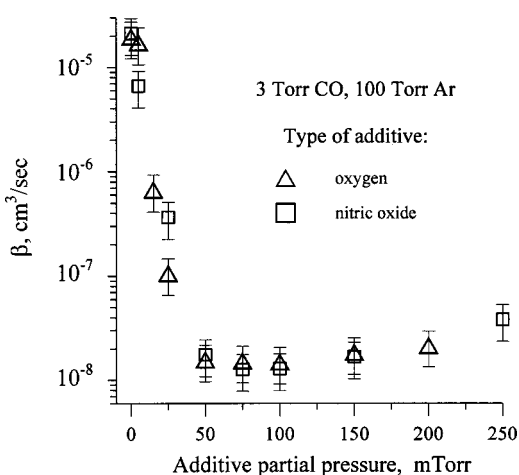


FIG. 13. Electron recombination rate coefficient in CO–Ar mixtures as a function of additive partial pressure.

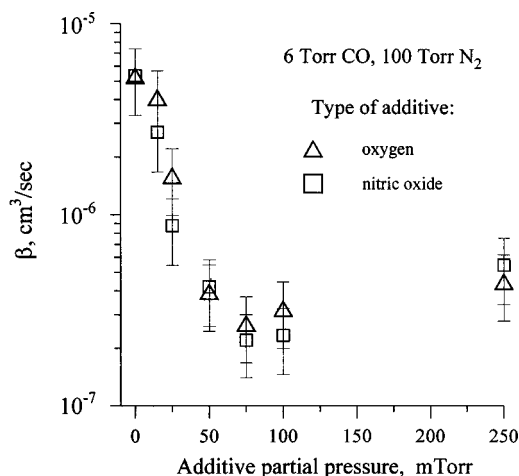
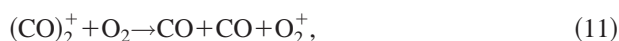


FIG. 14. Electron recombination rate coefficient in CO–N₂ mixtures as a function of additive partial pressure.

additives in the cell to $\beta \sim (2 \text{ to } 3) \times 10^{-7} \text{ cm}^3/\text{s}$ with 75–100 mTorr O₂ or NO added (see Fig. 14). Here again the difference between the recombination coefficients in O₂ and NO doped CO–N₂ mixtures is small.

Thus adding small amounts ($\sim 0.05\% - 0.1\%$) of O₂ and NO to the optically pumped CO–Ar and CO–N₂ plasmas allows control and considerable increase of the electron density [from $n_e = (6 - 8) \times 10^9 \text{ cm}^{-3}$ up to $n_e = (1 - 3) \times 10^{11} \text{ cm}^{-3}$] by reducing the electron–ion recombination rate (by up to 2 to 3 orders of magnitude). This result is consistent with the electron density and recombination rate inference from the rf probe plasma conductivity measurements.²⁰

Quantitative interpretation of the observed effect, i.e., identifying specific kinetic processes responsible for the electron recombination rate reduction, requires knowledge of the ion composition of the optically pumped plasma. However, a qualitative scenario can be suggested based on previous ion composition measurements in a glow discharge in CO–Ar–O₂ mixtures using *in situ* ion mass spectrometry.²⁶ The mass spectra taken in CO/Ar mixtures without oxygen show that the dominant ions in the discharge are dimer ions (CO)₂⁺ and cluster ions of the general form C_n(CO)₂⁺, $n = 1 - 15$. However, adding a few tens of millitorr of O₂ to these gas mixtures resulted in the nearly complete disappearance of these ions and their replacement by the O₂⁺ ions. Note that the electron–ion dissociative recombination rate of the dimer (CO)₂⁺ ion, $\beta = 2 \times 10^{-6} \text{ cm}^3/\text{s}$,²⁷ greatly exceeds the rate of recombination of the monomer O₂⁺ ion, $\beta = (3 - 5) \times 10^{-8} \text{ cm}^3/\text{s}$ at the electron temperature of $T_e \sim 0.3 - 0.5 \text{ eV}$.²¹ The recombination rate of the large carbon cluster ions can possibly be even higher. A similar process, i.e., destruction of the rapidly recombining carbon-based cluster ions and their replacement by the slowly recombining monomer ions, such as O₂⁺ and NO⁺, might also occur in optically pumped plasmas. This might occur in rapid exothermic ion–molecule reactions, such as





(both O_2 and NO have much lower ionization potential than CO). In addition, rapid resonance charge transfer from the vibrationally excited $\text{O}_2(v)$ and $\text{NO}(v)$ molecules to O_2^+ and NO^+ ions can produce vibrational excitation of these ions, which may further reduce the dissociative recombination rate.²⁸ More information on the detailed kinetic mechanism of the observed effect is expected to be obtained from ion mass spectrometry measurements in the optically pumped plasmas.

The observed effects also open a possibility of additional energy coupling to the vibrational modes of diatomic molecules in the optically pumped plasmas (such as CO and N_2). This process, which requires some initial ionization of the gas mixture, relies on free electron heating by an external sub-breakdown rf field with subsequent vibrational excitation by electron impact. Indeed, if the reduced electric field is in the range $E/N = (1-3) \times 10^{-16} \text{ V cm}^2$, which is about an order of magnitude lower than the breakdown threshold, up to 90% of the input electrical power coupled to the plasma goes to excitation of vibrational modes of molecules, such as CO and N_2 .²⁹⁻³¹ The use of this effect would allow sustaining large volumes of strongly nonequilibrium optically pumped gases without using a high-power pump laser.

IV. SUMMARY

Electron production rate and electron density in cold optically pumped CO-Ar and CO-N_2 plasmas in the presence of small amounts of O_2 and NO have been measured using a Thomson discharge probe and microwave attenuation. Nonequilibrium ionization in the plasmas is produced by an associative ionization mechanism in collisions of highly vibrationally excited CO molecules. It is shown that adding small amounts of O_2 or NO (50–100 mTorr) to the baseline gas mixtures at $P = 100$ torr results in an increase of the electron density by up to a factor of 20–40 (from $n_e < 10^{10}$ to $n_e = (1.5-3.0) \times 10^{11} \text{ cm}^{-3}$). This occurs while the electron production rate either decreases (as in the presence of O_2) or remains nearly constant within a factor of 2 (as in the presence of NO). It is also shown that the electron-ion recombination rates inferred from these measurements decrease by 2 to 3 orders of magnitude compared to their baseline values (with no additives in the cell), down to $\beta \cong 1.5 \times 10^{-8} \text{ cm}^3/\text{s}$ with 50–100 mTorr of oxygen or nitric oxide added to the baseline CO-Ar mixture, or $\beta \cong (2 \text{ to } 3) \times 10^{-7} \text{ cm}^3/\text{s}$ with 75–100 mTorr of O_2 or NO added to the baseline CO-N_2 mixture. The overall electron-ion removal rates in the presence of equal amounts of O_2 or NO additives turn out to be very close, which shows that the effect of electron attachment to oxygen at these conditions is negligible. These results suggest a novel method of electron density control in cold laser-sustained steady-state plasmas and open a possibility of sustaining stable high-pressure nonequilibrium plasmas at high electron densities and low plasma power budget.

ACKNOWLEDGMENTS

This research was supported in part by the Director of Defense Research and Engineering (DDR&E) within the Air Plasma Ramparts MURI Program managed by AFOSR, and by NSF/DOE "Partnership in Basic Plasma Science and Engineering" Program. Partial support from the Ohio Board of Regents Investment Fund is gratefully acknowledged. The authors would also like to express their sincere gratitude to Dr. J. Roscoe for his advice and assistance in development of microwave diagnostics, as well as to Professor Yu. Z. Ionikh for numerous useful discussions.

- ¹J. W. Rich, in *Applied Atomic Collision Physics*, edited by E. W. McDaniel and W. L. Nighan (Academic, New York, 1982), Vol. 3, pp. 99–1407.
- ²B. F. Gordiets, V. A. Osipov, and L. A. Shelepin, *Kinetic Processes in Gases and Molecular Lasers* (Gordon and Breach, London, 1988).
- ³J. W. Rich, R. C. Bergman, and M. J. Williams, Final Contract Report No. AFOSR F49620-77-C-0020, 1979 (unpublished).
- ⁴J. W. Rich and R. C. Bergman, *Chem. Phys.* **44**, 53 (1979).
- ⁵R. L. DeLeon and J. W. Rich, *Chem. Phys.* **107**, 283 (1986).
- ⁶C. Flament, T. George, K. A. Meister, J. C. Tufts, J. W. Rich, V. V. Subramaniam, J.-P. Martin, B. Piar, and M.-Y. Perrin, *Chem. Phys.* **163**, 241 (1992).
- ⁷H. L. Wallaart, B. Piar, M. Y. Perrin, and J. P. Martin, *Chem. Phys.* **196**, 149 (1995).
- ⁸E. Plönjes, P. Palm, A. P. Chernukho, I. V. Adamovich, and J. W. Rich, *Chem. Phys.* **256**, 315 (2000).
- ⁹H. Dünnwald, E. Siegel, W. Urban, J. W. Rich, G. F. Homicz, and M. J. Williams, *Chem. Phys.* **94**, 195 (1985).
- ¹⁰S. Saupe, I. Adamovich, M. J. Grassi, and J. W. Rich, *Chem. Phys.* **174**, 219 (1993).
- ¹¹D. S. Anex and G. E. Ewing, *J. Phys. Chem.* **90**, 1604 (1986).
- ¹²R. S. Disselkamp and G. E. Ewing, *J. Phys. Chem.* **93**, 6334 (1989).
- ¹³J. P. Galaup, J. Y. Harbec, R. Charneau, and H. Dubost, *Chem. Phys. Lett.* **120**, 188 (1985).
- ¹⁴I. Hadj Bachir, R. Charneau, and H. Dubost, *Chem. Phys.* **177**, 675 (1993).
- ¹⁵E. Plönjes, P. Palm, W. Lee, M. D. Chidley, I. V. Adamovich, W. R. Lempert, and J. W. Rich, *Chem. Phys.* **260**, 353 (2000).
- ¹⁶W. Lee, I. V. Adamovich, and W. R. Lempert, *J. Chem. Phys.* **114**, 1178 (2001).
- ¹⁷L. S. Polak, P. A. Sergeev, and D. I. Slovetskii, *High Temp.* **15**, 15 (1977).
- ¹⁸I. Adamovich, S. Saupe, M. J. Grassi, O. Schulz, S. Macheret, and J. W. Rich, *Chem. Phys.* **173**, 491 (1993).
- ¹⁹I. V. Adamovich and J. W. Rich, *J. Phys. D* **30**, 1741 (1997).
- ²⁰E. Plönjes, P. Palm, I. V. Adamovich, and J. W. Rich, *J. Phys. D* **33**, 2049 (2000).
- ²¹Y. P. Raizer, *Gas Discharge Physics* (Springer-Verlag, Berlin, 1991).
- ²²G. D. Billing, *Nonequilibrium Vibrational Kinetics* (Springer-Verlag, Berlin, 1986), Chap. 4, pp. 85–111.
- ²³S. Saupe, I. Adamovich, M. J. Grassi, and J. W. Rich, *Chem. Phys.* **174**, 219 (1993).
- ²⁴H. S. W. Massey, E. H. S. Burhop, and H. B. Gilbody, *Electronic and Ionic Impact Phenomena* (Clarendon, Oxford, 1971), Vol. 3.
- ²⁵E. W. McDaniel, *Collision Phenomena in Ionized Gases* (Wiley, New York, 1964).
- ²⁶Y. Kaufman, P. Avivi, F. Dothan, H. Keren, and J. Malinowitz, *J. Chem. Phys.* **72**, 2606 (1980).
- ²⁷R. Johnsen, in *Dissociative Recombination*, edited by B. R. Rowe *et al.* (Plenum, New York, 1993).
- ²⁸T. Mostefaoui, S. Laube, G. Gautier, C. Rebrion-Rowe, B. R. Rowe, and J. B. A. Mitchell, *J. Phys. B* **32**, 5247 (1999).
- ²⁹N. L. Aleksandrov, A. M. Konchakov, and E. E. Son, *Sov. J. Plasma Phys.* **4**, 169 (1978).
- ³⁰N. L. Aleksandrov, A. M. Konchakov, and E. E. Son, *Sov. Phys. Tech. Phys.* **49**, 661 (1979).
- ³¹N. L. Aleksandrov, F. I. Vysikailo, R. Sh. Islamov, I. V. Kochetov, A. P. Napartovich, and V. G. Pevgov, *High Temp.* **19**, 22 (1981).